JMEPEG (2025) 34:5652–5662
https://doi.org/10.1007/s11665-024-09581-6

1059-9495/$19.00

ORIGINAL RESEARCH ARTICLE

Comparison of Wear Behavior of Basic Oxygen Furnace Slag and WC-CoCr Coating

Dervis Ozkan, Ahmet Gulec, Mecit Oge, Yasin Ozgurluk, Gulfem Binal, Ibrahim Calis, Sefa Emre Sunbul, Mustafa Kaplan, Mustafa Sabri Gok, Yildiz Yarali Ozbek, Garip Erdogan, Sefa Erdem Yilmaz, Okan Odabas, Elif Olgun, and Abdullah Cahit Karaoglanli

Submitted: 4 August 2023 / Revised: 3 December 2023 / Accepted: 30 December 2023 / Published online: 28 May 2024

Metallurgical slags can be re-evaluated depending on their structural properties for reuse in many industrial applications. This study investigated the possibility of reusing these slags as a commercial value. The results of benchmark research comparing the friction and wear behavior of basic oxygen furnace slag (BOFS) and commercial wear-resistant coating against an Al_2O_3 counter body under dry conditions are presented in this work. Reciprocating wear tests were carried out on WC-CoCr, and slag coatings were deposited on 316L stainless steel substrates under different loads and sliding speeds. The wear track surfaces were compared using a scanning electron microscope (SEM), energy dispersive spectroscopy (EDS), and a 3D optical profilometer for wear-depth and wear-loss measurements. As a result of the experimental studies carried out, it was observed that BOFS coatings exhibited an appealingly superior wear performance. The study results showed that coatings with BOFS content could be used as an alternative candidate coating material equivalent to the wear-resistant coatings used in commercial and industrial areas in terms of performance.

Keywords atmospheric plasma spraying (APS), basic oxygen furnace slag (BOFS), high-velocity oxy-fuel spraying (HVOF), WC-CoCr, wear

1. Introduction

When an engineering component's surface is unable to adequately withstand the external factors or environment to which it is subjected, failures frequently occur. The main elements determining the lifespan of most machine components are degradation events like wear, corrosion, oxidation, and erosion (Ref 1). Surface improvements made possible by coating technologies extend the life span of components while protecting the substrate material and lowering replacement costs by delaying material deterioration (Ref 2). Thermal spraying is a significant coating technology applied in different industrial areas to protect materials and impart various physical-chemical properties to their surfaces (Ref 3). The thermal spray coating process involves rapidly heating the coating material in a hot gas atmosphere before applying it at high speed to the substrate surface to deposit the desired thickness (Ref 4). Thermal spray methods vary and are categorized according to the feedstock and heat source types (Ref 5). Due to its outstanding properties, including its low oxide content, low percentage of porosity, excellent hardness, fracture toughness, and bond strength, the HVOF spray method has been extensively utilized to deposit protective coatings on gas turbine blades and aerospace parts (Ref 6). Using the HVOF process, WC-CoCr coatings with good toughness, corrosion, and wear resistance are manufactured as hard surface coatings (Ref 7, 8). HVOF has special qualities, such as higher velocities and a lower flame temperature, which reduce WC decomposition during spraying, making it an ideal method for depositing WC-Co cermet coatings (Ref 9). The hard tungsten carbide (WC) phase and a softer CoCr metal matrix comprise the WC-CoCr cermet coating structure (Ref 7, 8). WC particles inside the coating show a high wear resistance during contact with surfaces, while adhesive strength and the ability to produce denser coatings are provided by CoCr (Ref 10). Dense HVOF-sprayed WC-CoCr cermets integrate high hardness with satisfactory toughness and good corrosion resistance (Ref 11, 12).

Regarding material manufacturing, high productivity and low production costs are crucial considerations. The industrial sector pays close attention to research using diverse wastes as feedstock sources. Basic oxygen furnace slag (BOFS) is a significant waste that occurs in enormous quantities in iron and

Dervis Ozkan, Mecit Oge, Mustafa Sabri Gok, Sefa Erdem Yilmaz, and **Okan Odabas**, Faculty of Engineering, Architecture and Design, Mechanical Engineering Department, Bartin University, 74110 Bartin, Turkey; **Ahmet Gulec**, Program of Machine and Welding Technology, Karasu Vocational School, Sakarya University of Applied Sciences, 54500 Sakarya, Turkey; **Yasin Ozgurluk**, Program of Medical Services and Techniques, Vocational School of Health Services, Bartin University, 74100 Bartin, Turkey; and **Gulfem Binal, Elif Olgun,** and **Abdullah Cahit Karaoglanli**, Faculty of Engineering, Architecture and Design, Metallurgical and Materials Engineering Department, Bartin University, 74110 Bartin, Turkey; **Ibrahim Calis**, Central Research Laboratory, Bartin University, 74110 Bartin, Turkey; **Sefa Emre Sunbul**, Faculty of Engineering, Metallurgical and Materials Engineering Department, Karadeniz Technical University, 61080 Trabzon, Turkey; **Mustafa Kaplan**, Vocational School, Departmant of Machinery and Metal Technologies, Metallurgy Program, Bilecik Seyh Edebali University, 11210 Bilecik, Turkey; **Yildiz Yarali Ozbek** and **Garip Erdogan**, Faculty of Engineering, Metallurgical and Materials Engineering Department, Sakarya University, 54050 Serdivan, Sakarya, Turkey. Contact e-mail: ozgurlukyasin@gmail.com.

Table 1 The HVOF spraying parameters of commercial hard metal coating

Powder	Combustion gases oxygen and kerosene, slpm and l/h	Carrier gas flow, L/min	Powder feed rate, g·min^{-1}	Stand-off distance, mm	Average coating thickness, μm
WC-CoCr	O_2 (800), CH_4 (25)	20	60	260	250-300

Table 2 The APS spraying parameters of BOFS coating

Powder	Current, A	Electrical power, kW	Feed rate, g·min^{-1}	Flow, L/min	Argon, pressure in MPa	H_2, pressure in MPa	Spray distance, mm
BOFS	600	40	30	4.5	0.5	0.1	110

Table 3 Deposition parameters of CoNiCrAlY coating using APS technique

Powder	Current, A	Electrical power, kW	Powder feed rate, g·min^{-1}	Argon flow rate, slpm	Hydrogen flow rate, slpm	Spray distance, mm
CoNiCrAlY	600	40	30	65	14	140

Table 4 Wear test parameters on APS and HVOF-sprayed coatings

Normal load, N	3-6-9
Sliding speed, m/s	0.12, 0.18
Total revolutions	18000
Data acquisition rate, Hz	2
Test temperature, °C	Room temperature
Counterface ball diameter, mm	6
Counterface ball hardness, HV_{10}	1500
Counterface ball material	Al_2O_3

steel plants and has not yet been fully utilized. BOFS is an industrial waste with pozzolanic characteristics, similar to fly ash. Different types of steelmaking slag are formed in steel production. BOFS slag is a dense, hard, and high-strength material. For this reason, it shows outstanding properties. It has been proven around the world that steelmaking slag can be used as ballast material, foundation material, and sub-base material on roads and railways. It has also been reported to be effective as anti-slip sand in sea filling and icing. BOFS is used as fertilizer raw materials. Research on the utilization of BOFS in the cement industry is also carried out (Ref 13, 14). According to their mass percentages, the primary oxides in BOF slag

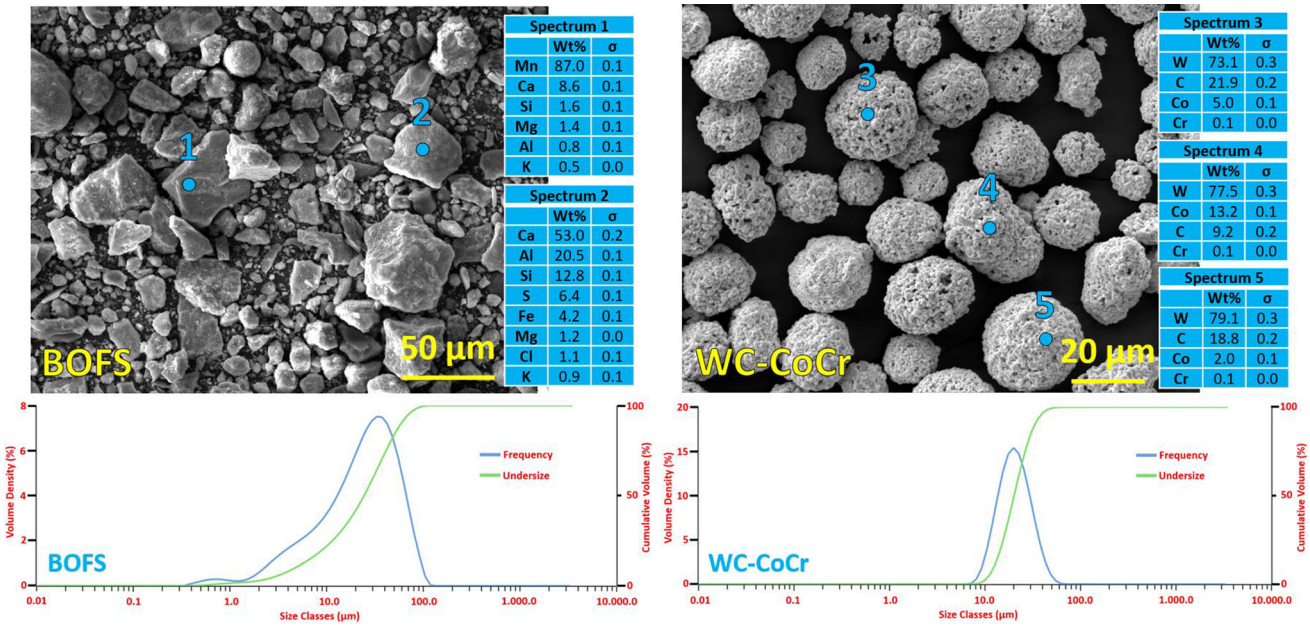

Fig. 1 Results of SEM microstructures, EDS, and particles size distribution analysis of the BOFS and WC-CoCr powder

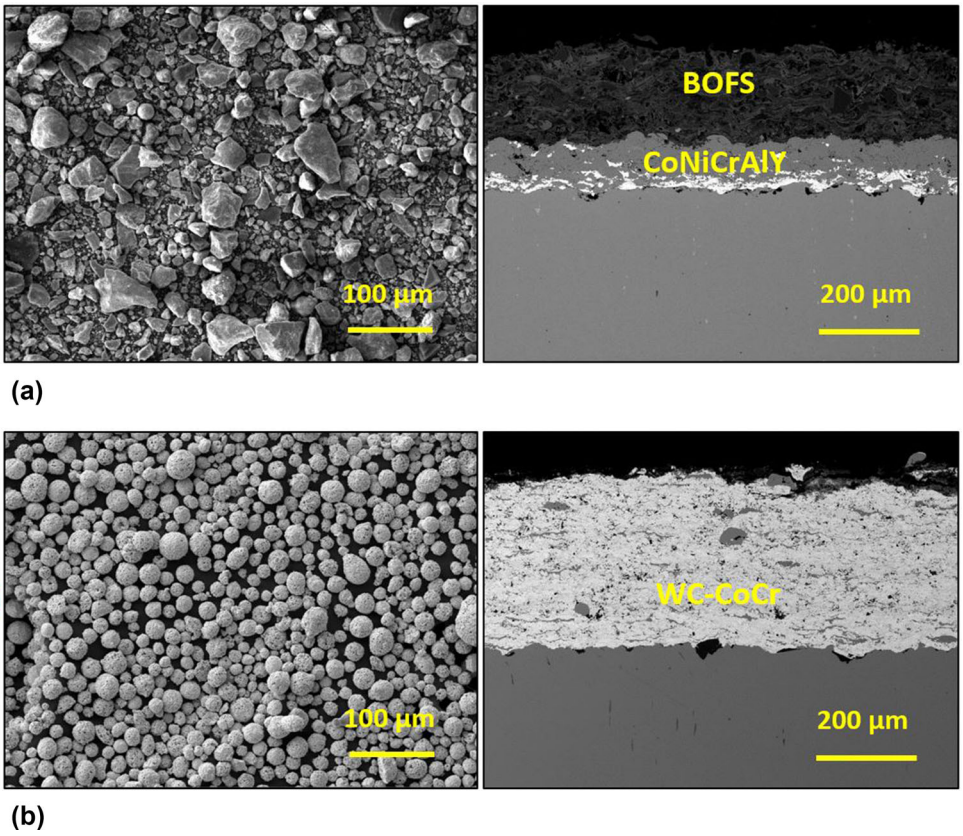

Fig. 2 SEM micrographs of the powders and cross-sectional microstructures of the as-deposited coatings; (a) BOFS and (b) WC-CoCr coating

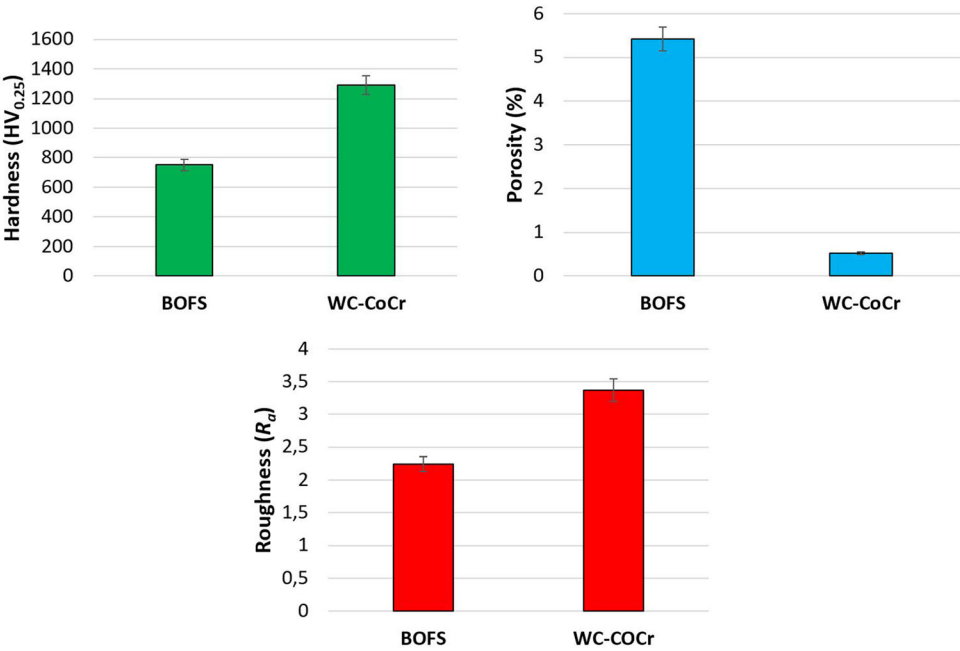

Fig. 3 Hardness, porosity, and surface roughness values of coatings after deposition process

(which contains heterogeneous oxides) include SiO_2, CaO, Al_2O_3, MgO, and Fe_2O_3 (Ref 15). Its ceramic-like structure makes BOFS a candidate thermal spray coating material. The chemical properties of the slag show that the atmospheric plasma spray (APS) coating method would be a good choice if BOFS was used as a coating material. Due to their high working temperature range, materials with a high melting point can be successfully deposited using the atmospheric plasma

spray (APS) method (Ref 16). Simple production, low cost, and high efficiency are the advantages of the APS method (Ref 17). This study aims to provide added value to waste material by researching the evaluation of basic oxygen furnace slag (BOFS) as a feedstock material for producing wear-resistant thermal spray coatings. For this purpose, BOFS was ground into coating powder and deposited on 316L stainless steel surfaces by the APS method. Commercial WC-CoCr powders were deposited on the 316L substrate using the HVOF method. Dry sliding wear tests under varied loads at room temperature were conducted to determine and compare the wear performances of the manufactured coatings.

2. Material and Methods

2.1 Coating Materials and Characterization

AISI 316 stainless steel, procured in round bar form and machined to the dimensions of 25 × 25 × 5 mm^3, was used as the substrate material for the coating system subjected to dry sliding wear tests. Commercially available WC-CoCr powders (GTV mbH-Germany, gas atomized and agglomerated) were used as the feedstock materials. Feedstock powders were heat treated at 80 °C in an open atmosphere furnace prior to deposition to remove humidity and improve flowability. Mechanically crushed BOFS in 2-3 mm particle size was granted by an iron-steel production company and further refined in a ball mill using Ø10-40 mm chrome-steel balls (65 HRC hardness) for 5 h and subjected to consecutive sieving to obtain an average particle size of 45-50 μm. Scanning electron microscopy (SEM) (Tescan MAIA3 XMU SEM, Czech Republic) and energy dispersive spectroscopy (EDS) analysis were utilized for microstructural investigations of powders, as well as sprayed and worn sample cross sections. Mean porosity data were calculated using the Image J software tool with the backscatter detector (BSD). Hardness measurements were applied to the revealed coating cross sections using a precision micro-hardness tester (Qness Q10, Austria) with a 250 g ($HV_{0.25}$) load and 15-s dwell time as the test parameters. 20 micro-hardness measurements were performed for each sample, and the mean values were used to evaluate the wear performance. The phase composition of the coatings was characterized using x-ray diffraction (Rigaku, Smartlab x-ray diffraction spectrometer). The particle size distributions of slags and commercial powders were verified by a Malvern Mastersizer 3000 (UK) particle sizer.

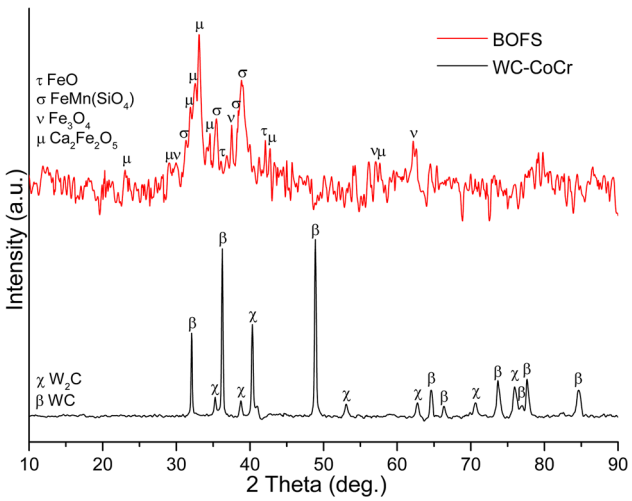

Fig. 4 XRD diffraction patterns of the BOFS and WC-CoCr coatings

Tribological commercial coating powders were deposited using the HVOF technique, while the BOFS powders were deposited using the APS technique due to their high melting points. An industrial HVOF gun (Hipojet 2700 M, India) and an APS gun with an MCN-type control unit were used for the deposition processes. HVOF parameters were selected in accordance with supplier information, whereas optimal APS parameters were achieved after a series of trials by the operator based on porosity and micro-hardness measurements. HVOF and APS deposition parameters were shown in Tables 1 and 2, respectively. The parameters used in the APS-sprayed MCrAlY coatings (F4-GTV, Germany) are shown in Table 3.

To eliminate the effect of initial surface roughness on wear performance, all samples subject to dry sliding wear tests were ground with SiC papers. The reciprocating mechanism of a hybrid (reciprocating-rotary) ball-on-disk tribometer (Turkyus Brand-Turkey) was used to measure the wear performance at room temperature under different loads and sliding speeds according to ASTM G133. The counter-face material properties and sliding wear parameters used during the tests are shown in Table 4. Wear volume losses were calculated using values based on the respective wear track. The wear rates were determined using the formula $w = V/(f \cdot l)$ $(m^3 \cdot (N \cdot m)^{-1})$, where V represents the wear volume (m^3), l represents the sliding distance (m), and f means the load (N).

When applying two different sliding speeds, the total number of revolutions of the test rig's spindle was kept constant at 18000 revolutions to apply the same number of contacts for each sliding speed parameter. Six test conditions (3 loads and 2 sliding speeds) were applied during the wear tests. The coefficient of friction (COF) rates were determined from the frictional forces (in grams) synchronously transferred from the load cell of the test rig to a personal computer in a log file, and COF versus revolution graphs were plotted accordingly. A Profilm3D brand (USA) 3D optical profilometer with sub-nanometer axial accuracy was used to obtain the worn volume data over a reciprocating distance of 1 cm. Each profilometer measurement was repeated five times to provide data reproducibility, and specific wear rate values in $m^3 \cdot (N \cdot m)^{-1}$ were calculated accordingly.

3. Results and Discussion

3.1 Powders and Coatings Characterization

The SEM images, EDS analysis, and the results of the particle size distribution analysis of BOFS and WC-CoCr powders are given in Fig. 1. BOFS has an angular and amorphous morphology with a Dv (50) particle size range of 24.4 μm. Also, the commercial coating powder of WC-CoCr has a Dv (50) particle size range of approximately 20.2 μm.

Figure 2 depicts the characteristic spherical morphology of agglomerated BOFS powder, and the coating has a uniform structure. APS technique was used to produce slag coating due to their composition and melting point. In this way, the slag

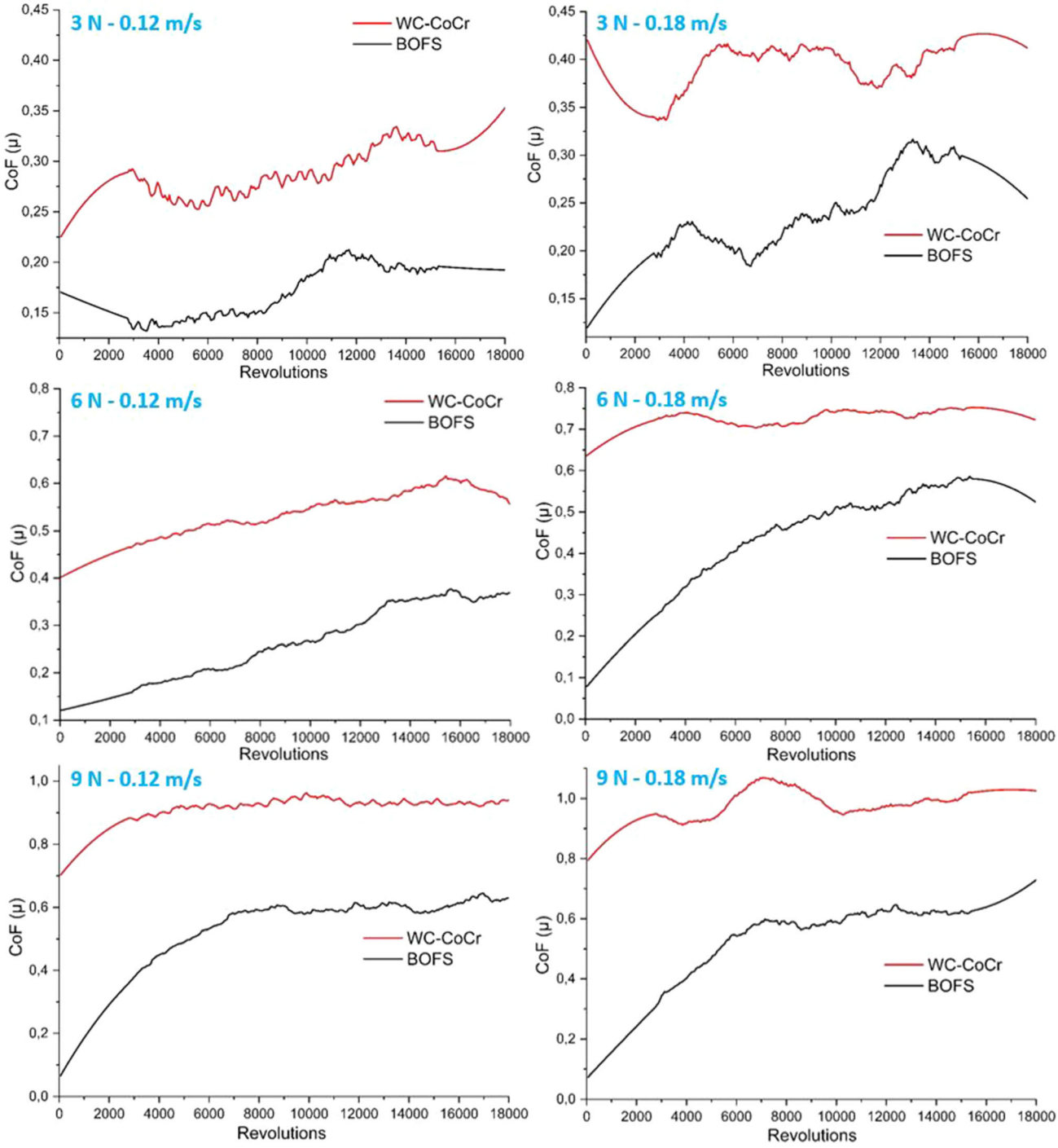

Fig. 5 Friction curves occurring in wear tests performed at varying test conditions

structures could be melted and coated on the substrate material surface. Due to the structural differences between the APS technique used in the production of slags compared to the HVOF technique, the microstructure of the slag coatings produced has more porosity and microcrack content than commercial WC-CoCr coating (Fig. 2). In addition, HVOF coatings have a more uniform microstructure content than APS coatings. Commercial wear-resistant HVOF coatings have similar coating thicknesses of 250-300 μm, while APS-sprayed BOFS coatings have coating thicknesses of 200-250 μm. The WC-CoCr particles are dispersed uniformly in the microstructures of the HVOF-sprayed coatings on the surface.

The results of the hardness $HV_{0.25}$ measurements of coatings are given in Fig. 3. It has been observed that the hardness of WC-CoCr coatings is high, depending on the WC particle reinforcements. Compared to WC-CoCr hard metal coating, BOFS coating has shown a low hardness value. Regarding surface roughness (R_a), the coating with the highest degree is WC-CoCr. Considering the porosity values, the coating with the highest porosity value is the BOFS coating.

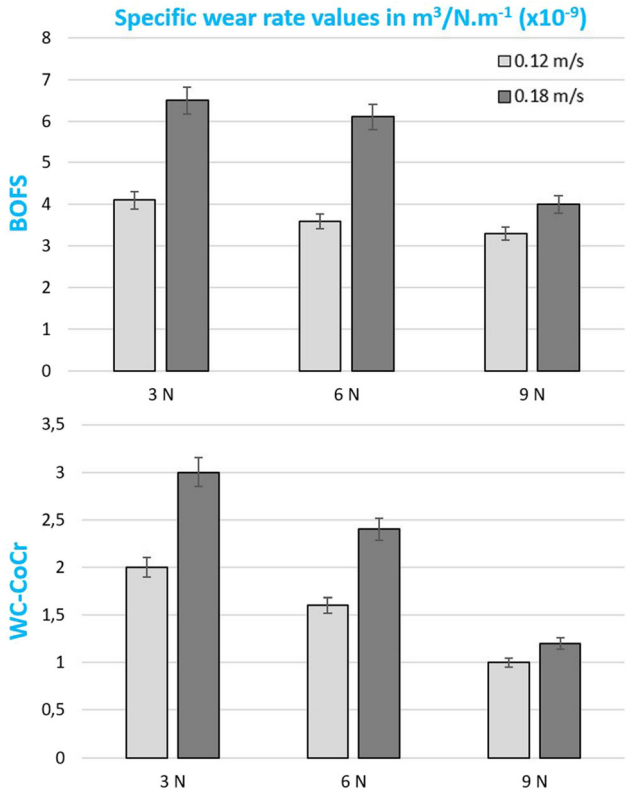

Fig. 6 Specific wear rates values of BOFS and WC-CoCr coatings under varying loads and sliding speeds

This situation occurs depending on the method used in producing BOFS coatings and the effect of the coating content.

Figure 4 demonstrates the XRD patterns of BOFS and WC-CoCr coating. The two principal iron oxides (FeO and Fe_3O_4) and fayalite–tephroite ($FeMn(SiO_4)$ are the main crystal structures for BOFS. The WC-CoCr coating's XRD pattern is dominated by WC peaks. Apart from WC, there is only a limited quantity of W_2C phase, demonstrating that the decarburization of nanostructured WC-Co-based powder can be effectively suppressed (Ref 18).

3.2 Wear Behavior of BOFS and WC-CoCr Coatings

Figure 5 illustrates the variation of average coefficient of friction (COF) values determined for the whole sliding distance and particular wear rates of HVOF commercial coating, and APS-sprayed BOFS coating under various loads and sliding speeds circumstances.

For both coatings, a transitory running-in stage exists at the start of the wear testing, as shown in Fig. 5, though it happens differently for each coating. This can be connected to the formation of tribo-oxidation products between asperity contact of the wear at an early stage and the severe micro-fracture and subsequent grain pull-out at a later stage of sliding (Ref 19, 20). It was observed that the CoF values of the BOFS coating were low at all loads. At a load of 3 N and a sliding speed of 0.12 m/s, an increase in the coefficient of friction up to 16000 revolutions was observed in both specimens, after which a transition to a stable state was observed. At the same shear rate of 9 N, it is seen that the transition to the stable state is faster. This can be attributed to the formation of an oxide layer with the temperature on the surface due to the increase in temperature between the interacting surfaces with increasing compression forces. This oxide layer stabilizes the graph, as it will form a compact and smooth structure with a higher hardness. However, the high CoF values at high loads are related to the roughness caused by the breakage of the oxide layer formed on the surface and the wear shown by the broken oxide layer. Furthermore, the WC-CoCr coating friction coefficient has a high noise during sliding wear, which is likely attributable to its higher surface roughness (Fig. 3). The friction coefficient of the BOFS was significantly elevated as the load was increased. The reason for this is that the BOFS's high porosities (Fig. 3) merge with stress micro-cracks that form during wear, causing more material separation from the body and increasing the friction coefficient. In addition, as seen in Fig. 3, there was a similar trend in the hardness and roughness values of both coatings. However, it was determined that such a clear trend was not observed in the CoF (Fig. 5). This means that the CoF is too complex to be associated only with hardness and roughness and can vary depending on the interaction of many mechanical parameters of the materials, such as hardness, toughness and elastic modulus (Ref 21).

It was observed that WC-CoCr exhibited a higher CoF value in the specimens under 9 N load with the increase in the shear rate, but it passed to a stable state faster, and BOFS also exhibited a more rigid CoF value curve. An applied normal load rised the coatings' wear rates independently of their sliding speed or temperature. Greater loads increase the frictional heat and the actual contact area at the interface leads to a higher wear rate. Increasing normal load and sliding speed demonstrate a similar effect on raising at the interface (Ref 22). On the other hand, the WC-CoCr coating's friction coefficient has increased during the wear test and has surpassed that of the BOFS coatings. When the WC-CoCr coating was subjected to a 9 N load, a severe friction coefficient occurred at the beginning of the dry sliding, movement of the ruptured and oxidized particles in the contact area enhanced the amount of wear. Friction coefficient fluctuation is correlated with the strength of the adhesive bond and the deformation that takes place during testing. The deformation that takes place during the experiment and the adhesion of the abraded material to the surface is the reasons behind the increasing trend of the friction coefficient. On the other hand, as the friction coefficient rises to high values, adhesive welding and bond breaking cause the friction coefficient to decrease.

Figure 6 shows the specific wear values of commercial WC-CoCr and BOFS specimens after a dry sliding test under different loads and at two different sliding speeds.

It is possible to say that commercial WC-CoCr shows superior wear resistance compared to BOFS. However, the wear resistance of the BOFS coating is also quite good in light of the values obtained. The high wear resistance of commercial WC-CoCr can be explained primarily by the hardness that occurs on the surface after coating. The hardness of the WC-CoCr specimen is 1293 ± 48.8 HV, while that of the BOFS specimen is 751 ± 27.4 HV (Fig. 3). Therefore, the WC-CoCr sample will show more resistance against the alumina ball with a hardness of 1500 HV, which wants to sink into it. Since this resistance will reduce the depth of abrasive penetration, the proportion of material deposited in front of the ball will also decrease. Thus, the wear rate will be relatively low. The decrease in wear rates with increasing load at the specified wear path distance can be explained as follows: During the tribological interaction, contact with the roughness is first

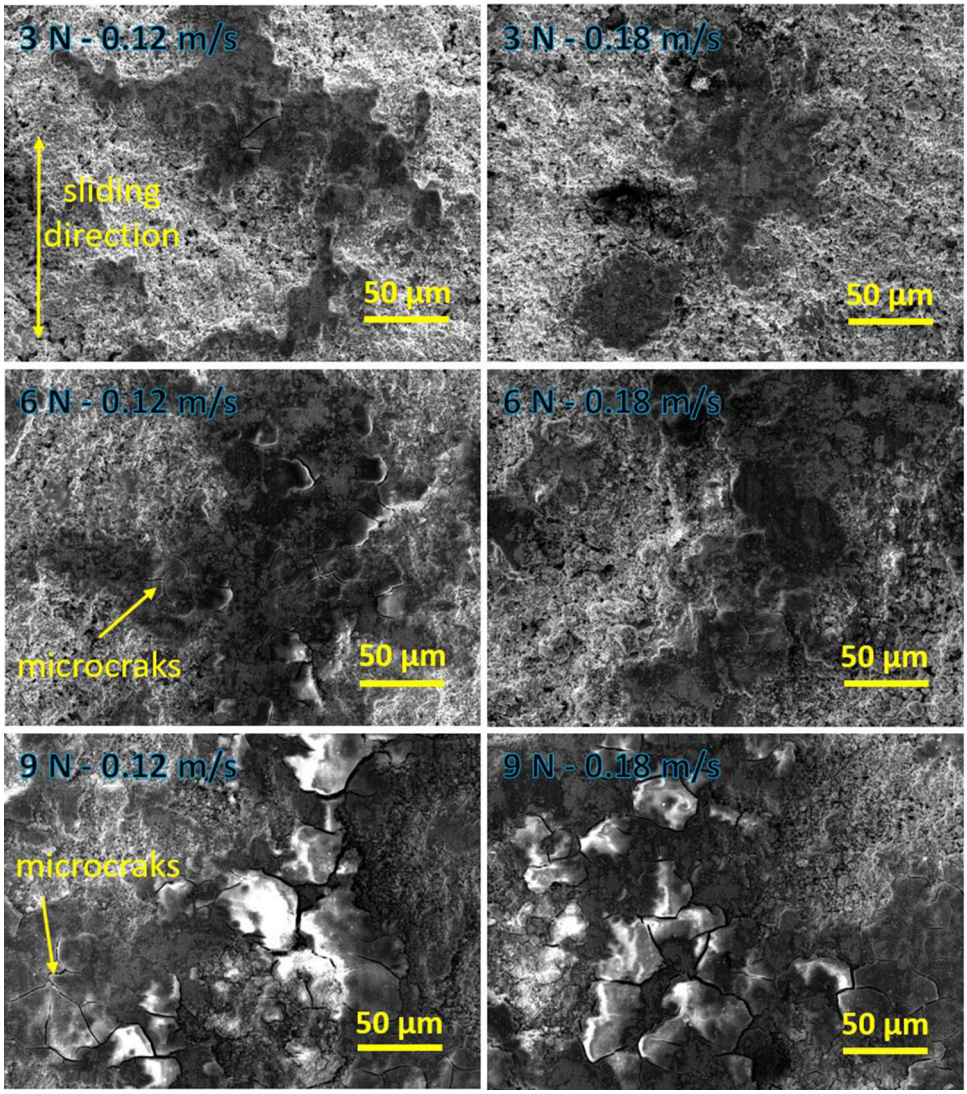

Fig. 7 SEM micrographs of wear traces of the WC-CoCr coatings under different test conditions

established between the surfaces. Under the influence of the compression and traction forces created by the ball, the rough peaks are cleaned, and wear wastes are formed. As a result of interaction and relative movement, some of these wastes are pushed out of the system, while some are filled into the gaps and roughnesses on the surface. In the meantime, as the interaction continues, both these wear wastes and the surface evolve into an oxidation-type wear mechanism. Increasing the load causes roughness and the surface to become more compact, and a smooth and slippery load-bearing oxide layer forms on the surface; thus, increasing the load causes volume losses to decrease to a certain extent. The chemical structure of the samples, tribological interaction parameters, and environment is important factors in the formation of this mechanism (oxidation) (Ref 23). After the oxide layers formed on the surface reach a certain thickness, it becomes a delamination-type wear mechanism with cracks forming on the surface and continuing under the surface. This mechanism was observed mainly at loads below 9N.

As the wear rates increase with the increase in speed, tangential shear stresses will occur due to the maximum compressive stress and the sliding force of the ball, along with the increasing load in the interaction zones and subsurface regions. These regressions will be effective in the plastic deformation of both the matrix and the coating area. Depending on the increasing load, the sliding mechanism, which forms the basis of the adhesive wear mechanism, will occur more actively. This will result in the formation of more wear particles. At much higher loads, higher shear stresses will accelerate plastic flow. In addition, compressive stress values will increase due to increasing load, which will cause crack nucleation in the surface area and the coating to break and fall off. It is also stated in the literature that particles broken off from the coating surface by abrasion will act as abrasive abrasives in the system (Ref 24-27).

The wear rates of the specimens increased approximately 1.5 times with increasing sliding speed. However, while this situation was observed, especially at 3 and 6 N loads, it was observed that the ratio changed less at a 9 N load compared to the others. Firstly, we can explain the increase in wear values at loads of 3 and 6 N with the increase in sliding speed as follows: At high shear rates, flash temperatures occur between the interacting surfaces. A positive benefit of this temperature rise is the formation of an oxide layer on the material's surface,

which improves wear resistance. However, depending on different parameters, this situation is not always realized at the desired level. It causes local thermal softening of the material with a high shear rate, a decrease in strength, and a reduction in hardness value due to thermal softening. This increases the wear of the specimen. The low wear values at high loads and high sliding speeds can be explained by the fact that the particles of the oxide layer formed on the surface, which become wear waste, form a tighter oxide layer on the surface by composing under a high load. Juanjuan et al. (Ref 28) stated that the sliding speed is the most important parameter affecting the wear rate between the applied sliding speed and applied pressure values.

SEM wear track images taken from the surfaces of WC-CoCr material at different loads and sliding speeds after the etching process are given in Fig. 7. At the load of 3N, the wear occurred in the local area at both sliding speeds, and the wear scar was not wholly formed. The peaks with high roughness were subjected to oxidation and delamination-type wear. Delamination wear occurs at the stages of crack formation, crack propagation, and merging with other cracks, resulting in material loss (Ref 29). Delamination wear, a type of fatigue wear, is caused by the continuous movement of surface roughnesses on each other at the sliding points. Small cracks occur under the surface. Due to the triaxial compressive stress just below the contact point, crack nucleation occurs. Continuous loading and deformation processes cause cracks to grow and merge with neighboring cracks (Ref 30). A similar situation is also seen in the SEM wear trace image in Fig. 7. It is observed that the cracks initiating under the surface, then perpendicular and parallel to the direction of sliding, grow together and cause damage. The heat generated during sliding causes oxidation on the worn surfaces. Oxygen penetration into the contact zone promotes the formation of different oxide layers. Therefore, the resulting oxide layer prevents metal-to-metal contact and causes a decrease in both wear rate and friction coefficient (Ref 31). It is seen that the wear trace expands with the increase in load to 6 and 9 N, especially at 9 N, where a complete wear trace is formed. Delamination and oxidation-type wear mechanisms were observed at both sliding speeds.

Recently, studies have focused on improving the mechanical and wear properties of WC-based wear-resistant coatings produced by the HVOF technique by choosing the suitable carbide and appropriately determining the other binder phases (Ref 32, 33). The worn surfaces of WC-CoCr samples under 9 N loads were examined by the SEM-EDS, and results are given in Fig. 8. The wear grooves are not visible, which is thought to be because the WC particles in the matrix support the matrix structure. As the load and speed increase, WC particles are seen more clearly on principle wear path, and it is seen that the Co, which forms the matrix structure, is separated from the surface by the adhesive wear mode along the wear path.

Wear trace SEM images taken from BOFS-coated samples, which were subjected to a dry sliding wear test with different processing parameters, are given in Fig. 9.

When the SEM wear surface images of BOFS coating are analyzed, it can be said that oxidation and delamination-type mechanisms are dominant. It is observed that the surface is rougher due to insufficient surface pressure at low loads and sliding speeds. It is seen that a smoother surface is formed with the heat generated on the surface with increasing speed. At high loads, the areas with a dark and smooth structure have a higher oxide content, and the rougher other regions are the subsurface that emerges after the broken oxide layers. It can be seen that with increasing load, the width of the trace increases, and micro-cracks are formed; however, with the increase in the load, plastic flow occurs in the shear direction. The dominant wear modes in the formation of delamination, fracture formation, and material loss from the surface can be seen in Fig. 9. It

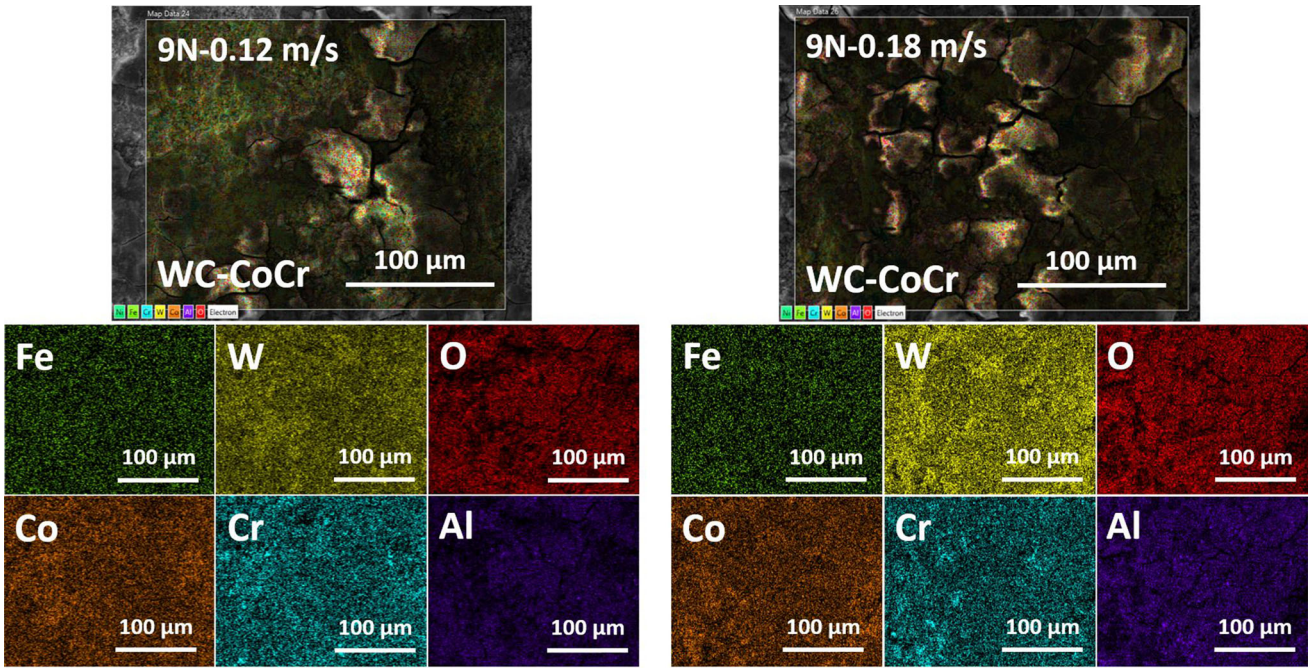

Fig. 8 SEM elemental mapping results of the wear tracks for WC-CoCr coating under 9 N load with different sliding speeds

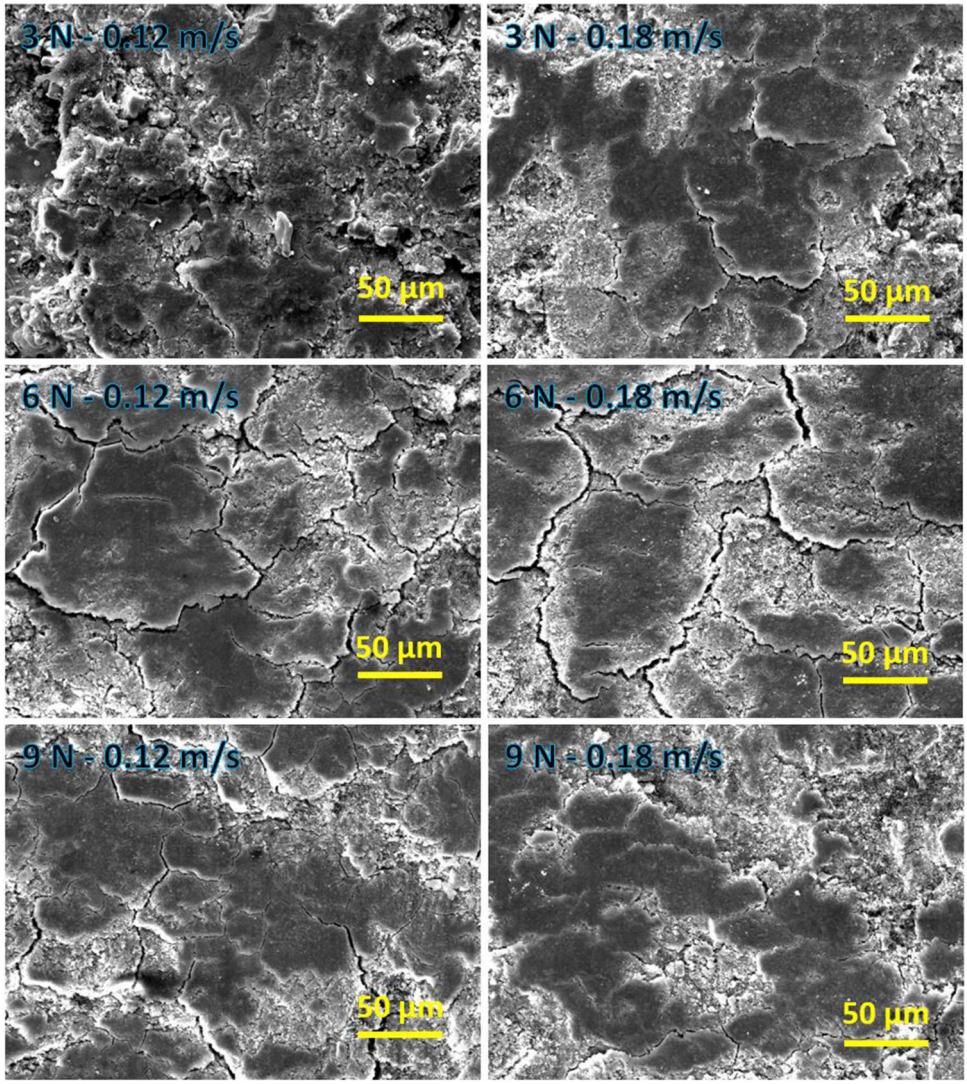

Fig. 9 SEM micrographs of wear traces of the BOFS under different test conditions

is also noticed that the laminates are separated from the surface in layers under the influence of tensile and compressive stresses during the wear process. Plastic flow occurring on the surface with tensile stresses caused local material loss from the BOFS surface. It is also seen that these layer separations spread toward the surface in contact with the ball over time.

The worn surfaces of BOFS samples were examined under 9 N loads by the SEM-EDS, and the results can be seen in Fig. 10. The BOFS coating, which has an oxide character, increased the wear rate by causing intense material loss in this way. While some wear particles are removed over time on contact surfaces where abrasive wear is involved, others become stuck in the wear trace channels on the surface, with the effect of fracture and plastic deformation. In addition, the superimposed debris is also oxidized on the BOFS coating.

In the study evaluated by Kumar et al. (Ref 34) on YSZ and WC-10Co-4Cr coatings, it was seen that the increase in hardness was directly proportional to the increase in nanoparticles in the coating. In the study where erosion behavior was evaluated, it was observed that the nanoparticles added at different rates increased the resistance and strength against erosion behavior. Similarly, in our study, it was observed that slag powders of different sizes showed higher hardness and strength compared to commercial coatings after the coating process. In another study by Kumar et al. (Ref 35) in which YSZ nanoparticles were reinforced into the WC-Co-Cr coating material coated on turbine steel, HVOF was used, similar to our study. In the study, solid particle abrasives were used as wear tests because the turbine blades operate at high temperatures. The effects of hot abrasive particles sent onto the work piece during the operation of the work piece were investigated. Similar to other studies in the literature, nanoparticles added to the coating material had an increasing effect on the strength of the turbine blades. Similar to this study, in our previous study in which the hot corrosion behavior of WC-Co-Cr commercial coating material was coated on 316L stainless steel and its hot corrosion behavior was investigated, it was observed that this coating material had some disadvantages at high temperatures. It is thought that WC-Co-Cr coatings produced by the HVOF method have good anti-wear behavior, but they should not be preferred at high temperatures (Ref 36).

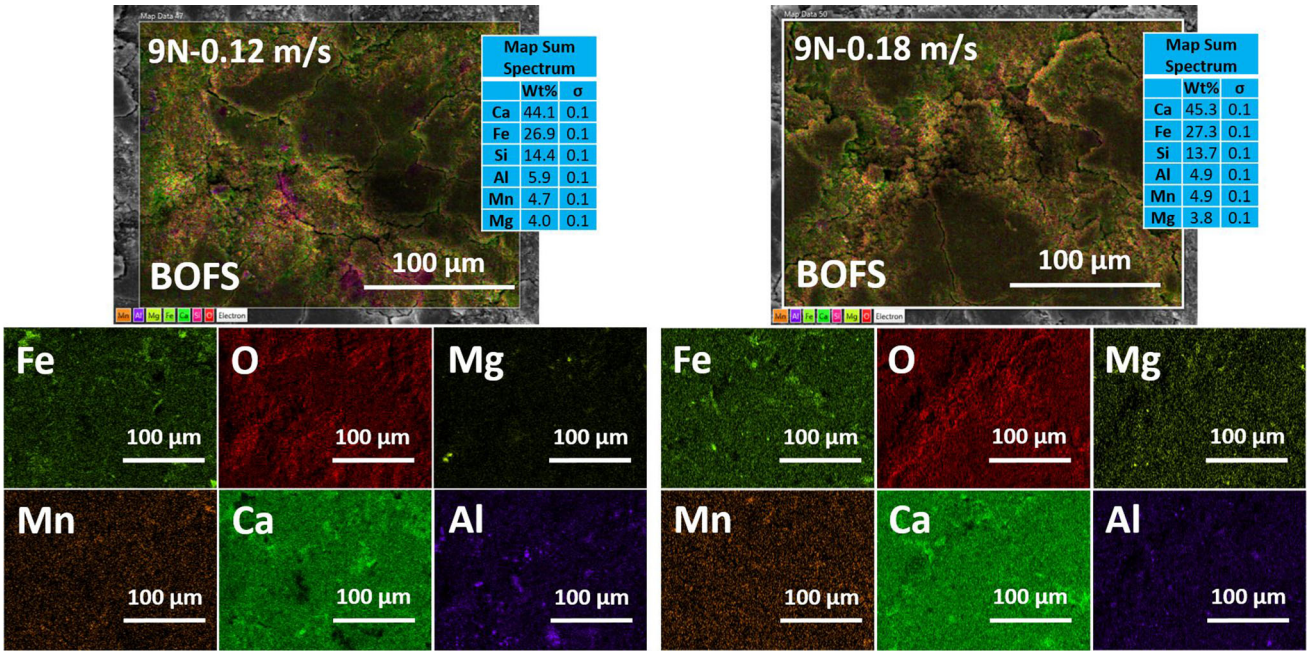

Fig. 10 SEM elemental mapping results of the wear tracks for BOFS coating under 9 N load with different sliding speeds

4. Conclusions

In this study, commercial wear-resistant WC-CoCr coatings were produced by HVOF, and slag material BOFS coatings were produced by APS techniques to compare wear performance and microstructural characteristics. To better understand the wear mechanisms, the coatings were subjected to wear tests under dry conditions with three different loads and two different sliding speeds. The findings obtained as a result of the study are given below.

- In the study, it was observed that the parameters determining the wear performance were the surface roughness, hardness, and microstructural characteristics of the thermal spray coatings subjected to the tests.
- The wear rate was the main parameter that increased the material losses of coatings on the contact surfaces.
- It has been observed that the wear load and sliding speed increases adversely affect all coatings. Frictional material loss increases with increasing load and sliding speed. The specific wear rates of the samples increased depending on the high sliding speed.
- Although BOFS coating has the highest porosity rate, it showed better wear performance than commercial coating with low porosity content produced by the HVOF technique.
- It has been observed that tribological layers and surface changes occur depending on the time in the microstructure of the coatings in both thermal spray coating techniques. Cracking and delamination-type wear mechanisms were observed on the surfaces of the samples subjected to dry sliding wear test due to thermal effect and compression force stresses.
- BOFS coatings, a slag waste product, can be used in different industrial applications due to their wear resistance. Future studies will focus on BOFS, which is an industrial waste material and the development of its use and qualities in thermal spray coating applications.

Acknowledgments

We are grateful for the financial support from the Scientific Research Projects (BAP) Coordinatorship of Bartin University with project numbers 2013.1.81 and 2015-FEN-F-001.

References

1. A.R. Govande, A. Chandak, B.R. Sunil, and R. Dumpala, Carbide-Based Thermal Spray Coatings: A Review on Performance Characteristics and Post-Treatment, *Int. J. Refract. Met. Hard Mater.*, 2022, **103**, 105772. https://doi.org/10.1016/j.ijrmhm.2021.105772
2. A.S.M. Ang, C.C. Berndt, and P. Cheang, Deposition Effects of WC Particle Size on Cold Sprayed WC-Co Coatings, *Surf. Coat. Technol.*, 2011, **205**, p 3260–3267. https://doi.org/10.1016/j.surfcoat.2010.11.045
3. C.J. Li, X.T. Luo, S.W. Yao, G.R. Li, C.X. Li, and G.J. Yang, The Bonding Formation during Thermal Spraying of Ceramic Coatings: A Review, *J. Therm. Spray. Tech.*, 2022, **31**, p 780–817. https://doi.org/10.1007/s11666-022-01379-z
4. K. Sunitha and H. Vasudev, A Short Note on the Various Thermal Spray coating Processes and Effect of Post-Treatment on Ni-Based Coatings, *Mater. Today Proc.*, 2022, **50**, p 1452–1457. https://doi.org/10.1016/j.matpr.2021.09.017
5. K. Derelizade, A. Rincon, F. Venturi, R.G. Wellman, A. Kholobystov, and T. Hussain, High Temperature (900 °C) Sliding Wear of CrNiAlCY Coatings Deposited by High Velocity Oxy Fuel Thermal Spray, *Surf. Coat. Technol.*, 2022, **432**, 128063. https://doi.org/10.1016/j.surfcoat.2021.128063
6. G. Prashar and H. Vasudev, A Review on the Influence of Process Parameters and Heat Treatment on the Corrosion Performance of Ni-Based Thermal Spray Coatings, *Surf. Rev. Lett.*, 2022, **29**, p 2230001. https://doi.org/10.1142/S0218625X22300015

7. P. Jayashree, S. Turani, and G. Straffelini, Effect of Velocity and Temperature on the Dry Sliding Behavior of a SiC-Graphite Composite Against WC-CoCr and WC-FeCrAlY HVOF Coatings, *Wear*, 2021, **464**, 203553. https://doi.org/10.1016/j.wear.2020.203553
8. M. Magnani, P.H. Suegama, A.A.C. Recco, J.M. Guilemany, C.S. Fugivara, and A.V. Benedetti, WC-CoCr Coatings Sprayed by high Velocity Oxygen-Fuel (HVOF) Flame on AA7050 Aluminum Alloy: Electrochemical Behavior in 3.5% NaCl Solution, *Mater. Res.*, 2007, **10**, p 377–385. https://doi.org/10.1590/S1516-14392007000400010
9. L. Thakur, N. Arora, R. Jayaganthan, and R. Sood, An Investigation on Erosion Behavior of HVOF Sprayed WC-CoCr Coatings, *Appl. Surf. Sci.*, 2011, **258**, p 1225–1234. https://doi.org/10.1016/j.apsusc.2011.09.079
10. G. Bolelli, L. Lusvarghi, and M. Barletta, HVOF-Sprayed WC-CoCr Coatings on Al Alloy: Effect of the Coating Thickness on the Tribological Properties, *Wear*, 2009, **267**, p 944–953. https://doi.org/10.1016/j.wear.2008.12.066
11. M. Barletta, G. Bolelli, B. Bonferroni, and L. Lusvarghi, Wear and Corrosion Behavior of HVOF-Sprayed WC-CoCr Coatings on Al Alloys, *J. Therm. Spray. Tech.*, 2010, **19**, p 358–367. https://doi.org/10.1007/s11666-009-9387-1
12. J.A. Picas, E. Rupérez, M. Punset, and A. Forn, Influence of HVOF Spraying Parameters on the Corrosion Resistance of WC-CoCr Coatings in Strong Acidic Environment, *Surf. Coat. Technol.*, 2013, **225**, p 47–57. https://doi.org/10.1016/j.surfcoat.2013.03.015
13. T.S. Naidu, C.M. Sheridan, and L.D. van Dyk, Basic Oxygen Furnace Slag: Review of Current and Potential Uses, *Minerals Eng.*, 2020, **149**, 106234. https://doi.org/10.1016/j.mineng.2020.106234
14. C. Kambole, P. Paige-Green, W.K. Kupolati, J.M. Ndambuki, and A.O. Adeboje, Basic Oxygen Furnace Slag for Road Pavements: A Review of Material Characteristics and Performance for Effective Utilization in Southern Africa, *Constr. Build. Mater.*, 2017, **148**, p 618–631. https://doi.org/10.1016/j.conbuildmat.2017.05.036
15. Y. Xue, H. Hou, and S. Zhu, Characteristics and Mechanisms of Phosphate Adsorption Onto Basic Oxygen Furnace Slag, *J. Hazardous Mater.*, 2009, **162**, p 973–980. https://doi.org/10.1016/j.jhazmat.2008.05.131
16. H. Kumar, G.A. Bhaduri, S.G.K. Manikandan, M. Kamaraj, and S. Shiva, Microstructural Characterization and Tribological Properties of Atmospheric Plasma Sprayed High Entropy Alloy Coatings, *J. Therm. Spray. Tech.*, 2022, **31**, p 1956–1974. https://doi.org/10.1007/s11666-022-01422-z
17. Q. Ding, X. Tan, L. Jiang, X. Fan, B. He, C. Wang, X. Zhuo, K. Zhou, and X. Zhang, High-Temperature Performances of Si-HfO_2-Based Environmental Barrier Coatings via Atmospheric Plasma Spraying Ceram, *Int.*, 2022, **48**, p 23127–23136. https://doi.org/10.1016/j.ceramint.2022.04.293
18. H. Wang, X. Wang, X. Song, X. Liu, and X. Liu, Sliding wear Behavior of Nanostructured WC-Co-Cr Coatings, *Appl. Surf. Sci.*, 2015, **355**, p 453–460. https://doi.org/10.1016/j.apsusc.2015.07.144
19. S. Hong et al., Improvement in Tribological Properties of Cr12MoV Cold Work die Steel by HVOF Sprayed WC-CoCr Cermet Coatings, *Coatings*, 2019, **9**(12), p 825
20. L. Wu et al., Reciprocating Friction and Wear Behavior of Ti_3AlC_2 and Ti_3AlC_2/Al_2O_3 Composites Against AISI52100 Bearing Steel, *Wear*, 2009, **266**(1–2), p 158–166
21. S.R. Medabalimi, M. Ramesh, and R. Kadoli, Developing Partially Oxidized NiCr Coatings Using the Combined Flame Spray and Plasma Spray Process for Improved Wear Behaviour at High Temperature, *Wear*, 2021, **478**, 203885
22. K. Torkashvand, V.K. Selpol, M. Gupta, and S. Joshi, Influence of Test Conditions on Sliding Wear Performance of High Velocity Air fuel-Sprayed WC-CoCr Coatings, *Materials*, 2021, **14**(11), p 3074
23. F. Hayat and C.T. Sezgin, Wear Behavior of Borided Cold-Rolled High Manganese Steel, *Coatings*, 2021, **11**(10), p 1207
24. A. Günen, Tribocorrosion Behavior of Boronized Co1.19Cr1.86-Fe1.30Mn1.39Ni1.05Al0.17B0.04 High Entropy Alloy, *Surf. Coat. Technol.*, 2021, **421**, p 127426
25. M. Kilic, D. Ozkan, M.S. Gok, and A.C. Karaoglanli, Room-and High Temperature Wear Resistance of MCrAlY Coatings Deposited by Detonation gun (D-gun) and Supersonic Plasma Spraying (SSPS) Techniques, *Coatings*, 2020, **10**(11), p 1107
26. G. Bolelli, L.M. Berger, M. Bonetti and L. Lusvarghi, Comparative Study of the Dry Sliding Wear Behaviour of HVOF-Sprayed WC-(W, Cr) 2C-Ni and WC-CoCr Hardmetal Coatings, *Wear*, 2014, **309**(1–2), p 96–111
27. F. Çavdar, A. Günen, E. Kanca, Y. Er, M.S. Gök, M. Ivan Campos-Silva, and M. IOlivares-Luna, An Experimental and Statistical Analysis on Dry Sliding Wear Failure Behavior of Incoloy 825 at Elevated Temperatures, *J. Mater. Eng. Perform.*, 2022, **32**(9), p 4161–4184. https://doi.org/10.1007/s11665-022-07381-4
28. Z. Juanjuan, M. Le, and R. Dwyer-Joyce, Friction and Wear Behaviors of Self-Lubricating Peek Composites for Articulating Pin Joints, *Tribol. Int.*, 2020, **149**, 105741. https://doi.org/10.1016/j.triboint.2019.04.025
29. S. Das, S.V. Prasad, and T.R. Ramachandran, Microstructure and Wear of Cast (Al-Si alloy)-Graphite Composites, *Wear*, 1989, **133**, p 173–187. https://doi.org/10.1016/0043-1648(89)90122-1
30. T.R. Prabhu, V.K. Varma, and S. Vedantam, Effect of SiC Volume Fraction and Size on Dry Sliding Wear of Fe/SiC/graphite Hybrid Composites for High Sliding Speed Applications, *Wear*, 2014, **309**, p 1–10. https://doi.org/10.1016/j.wear.2013.10.006
31. B. Venkataraman and G. Sundararajan, Correlation Between the Characteristics of the Mechanically Mixed Layer and Wear Behaviour of Aluminum, Al-7075 Alloy and Al-MMCs, *Wear*, 2000, **245**, p 22–38. https://doi.org/10.1016/S0043-1648(00)00463-4
32. S. Hong, Y. Wu, B. Wang, and J. Lin, Improvement in Tribological Properties of $Cr_{12}MoV$ Cold Work Die Steel by HVOF Sprayed WC-CoCr Cermet Coatings, *Coatings*, 2019, **9**, p 825. https://doi.org/10.3390/coatings9120825
33. A. Mateen, G.C. Saha, T.I. Khan, and F.A. Khalid, Tribological Behaviour of HVOF Sprayed Near-Nanostructured and Microstructured WC-17 wt.% Co Coatings, *Surf. Coat. Technol.*, 2011, **206**, p 1077–1084. https://doi.org/10.1016/j.surfcoat.2011.07.075
34. R. Kumar, K. Goyal, and D. Bhandari, Slurry Erosion Behavior of Thermally Sprayed Nano YSZ Reinforced WC-10Co-4Cr Ceramic Nanocomposite Coatings, *Tribol. Trans.*, 2023, **66**(1), p 47–58
35. R. Kumar, D. Bhandari, and K. Goyal, Mechanical and Microstructural Characterization of Yttria-Stabilized Zirconia (Y_2O_3/ZrO_2; YSZ) Nanoparticles Reinforced WC-10Co-4Cr Coated Turbine Steel, *J. Electrochem. Sci. Eng.*, 2022, **12**(4), p 651–666
36. Y. Ozgurluk, Evaluation of Hot Corrosion Behavior of WC-Co-Cr Coatings Coated by the HVOF Method, *J. Mater. Mechatron. A*, 2023, **4**(1), p 286–301